INTERNATIONAL JOURNAL OF HYDROGEN ENERGY 44 (2019) 3553–3559

Available online at www.sciencedirect.com

ScienceDirect

journal homepage: www.elsevier.com/locate/he

Short Communication

A continuous valence band through N–O orbital hybridization in N–TiO_2 and its induced full visible-light absorption for photocatalytic hydrogen production

Shuchao Sun [a,b], *Qianqian Chi* [a], *Han Zhou* [a], *Wei Ye* [a,*], *Genping Zhu* [a], *Peng Gao* [a,*]

[a] *College of Material, Chemistry and Chemical Engineering, Hangzhou Normal University, Hangzhou, Zhejiang, 311121, PR China*

[b] *School of Materials Science and Engineering, Harbin Institute of Technology, Harbin, Heilongjiang, 150001, PR China*

ARTICLE INFO

Article history:
Received 2 October 2018
Received in revised form
14 December 2018
Accepted 15 December 2018
Available online 6 January 2019

Keywords:
Continuous valence band
Orbital hybridization
photocatalytic
Hydrogen production

ABSTRACT

Photocatalytic hydrogen production represents an effective approach for solar energy conversion, which can greatly ease the current energy crisis. Herein, we report a successful N–O orbital hybridization in N-doped TiO_2 nanotube, the absorption wavelength is greatly red-shifted to visible light (from 400 to 800 nm) with large absorbance. The doping N element can partially replace the oxygen sites in TiO_2 lattice to form N–Ti–N bonds. The hybridization effect of N 2p and O 2p makes a continuous valence band and the position up-shift from 1.99 to 1.67 eV, the band gap is subsequently narrowed from 3.21 to 2.77 eV for 1.85-N–TiO_2 nanotube, which has been confirmed by ultraviolet–visible diffuse reflectance spectra and X-ray photoelectron spectroscopy valence band spectra. Benefiting from the enhanced visible light absorption ability and ultrathin shell feature, 1.85-N–TiO_2 nanotube exhibits exciting photocatalytic hydrogen evolution performance with a rate of 10870 μmol h^{-1} g^{-1} under the selected visible light irradiation ($\lambda > 400$ nm). This work demonstrates an alternative strategy for tuning visible light absorption ability by doping for wide-band-gap semiconductors in photocatalysts design, and the philosophy can also be extended to other photocatalytic systems.

© 2018 Hydrogen Energy Publications LLC. Published by Elsevier Ltd. All rights reserved.

* *Corresponding authors*. College of Material, Chemistry and Chemical Engineering, Hangzhou Normal University.
E-mail addresses: yewei@hznu.edu.cn (W. Ye), gaopeng@hrbeu.edu.cn (P. Gao).

https://doi.org/10.1016/j.ijhydene.2018.12.097

0360-3199/© 2018 Hydrogen Energy Publications LLC. Published by Elsevier Ltd. All rights reserved.

Introduction

Titanium dioxide (TiO_2), as a prominent photocatalyst in solar energy conversion [1,2], has been significantly regarded as a candidate for generating hydrogen through photocatalytic process due to its plentiful, efficient and stable merits in aqueous solution [3–5]. However, it is a typical wide-band-gap semiconductor (3.2 eV for anatase phase) and mainly absorbs ultraviolet light (290–400 nm), this greatly limits its actual catalytic applications as ultraviolet light only accounts for 8.7% of sun light [6]. To date, non-metallic element doping in TiO_2, such as N, S, C etc., has been proved an extremely effective method in narrowing its band gap to maximize visible light absorption [7–11]. The exact reason is that their 2p orbit is intercalated above the pristine O 2p in the band gap and results in the following up-shift of the valence band edge in TiO_2 [12–15]. In previous experimental works about N-doped TiO_2, most of them only realized the formation of interstitial N-doping [16–19], which almost kept the valence band edges unchanged with poor visible-light absorption ability and also brought new recombination centers to aggravate the quantum efficiency loss [20]. It is gratifying that recent theoretical calculations revealed that the substitutional N in oxygen sites could form a continuous valence band, which was composed of the hybrid orbits of N 2p and O 2p, and it can greatly extend the light absorption to visible-light region [21–23]. However, as N-doping will introduce new recombination centers, so an efficient electron-hole separation is needed. It was proved that the carrier trapping ability at the N-induced sites is crystallography dependent [24]. For example: The hole trapping probability is raised when the photogenerated holes diffuse along ⟨110> and ⟨001> directions, and the detrapping probability increases if the holes diffuse along <100⟩ direction. Therefore, N-doped TiO_2 nanocrystals with specific facet may maintain comparable electron/holes separation efficiency.

Herein, we selected hollow anatase phase TiO_2 nanotube bounded by rolled (101) facet as the precursor to construct substitutional N-doped TiO_2 nanotube through a simple solvothermal method. The light absorption range of TiO_2 nanotubes were extended to visible-light after successful N-doping. 1.85-N–TiO_2 sample achieved a striking H_2 production rate of 10870 μmol h^{-1} g^{-1} under visible-light irradiation, well exceeding the performance of other TiO_2-based nanocrystals (Table 1).

Experimental

Synthesis of 1.85-N–TiO₂ nanotube. 0.2 g of pristine TiO_2 nanotube was firstly dispersed into a mixture containing 12 mL absolute ethanol and 8 mL deionized water in a 50 mL glass beaker. After that, 20 mL of 28–30% $NH_3 \cdot H_2O$ was added under stirring. After 2 h, the mixture was transferred into a 50 mL Teflon autoclave and then it was sealed. The autoclave was placed in an oven and maintained at 180 °C for 15 h. After naturally cooled to room temperature, the sample was collected with centrifugation and rinsed with ethanol/water mixture several times. Finally, the as-obtained products were calcined at 500 °C for 2 h under Ar atmosphere in the tube furnace. The procedures for N-doped TiO_2 samples with varied N contents were similar with 1.85-N–TiO_2 nanotube except for different $NH_3 \cdot H_2O$ amount. For example, the actual volumes of $NH_3 \cdot H_2O$ for 0.95-N–TiO_2, 1.04-N–TiO_2, 1.28-N–TiO_2, 2.51-N–TiO_2, 3.53-N–TiO_2 nanotubes were 5 mL, 10 mL, 15 mL, 25 mL and 30 mL, respectively.

Photocatalytic hydrogen production. The photocatalytic hydrogen evolution reaction was performed using a commercial online photocatalytic hydrogen production system (AuLight, Beijing, CEL-SPH2N). Specifically, 0.1 g of 1.85-N–TiO_2 nanotube was added into a 100 mL aqueous solution containing 80 mL water, 20 mL methanol in a quartz reactor. Then, a few drops of chloroplatinic acid solution (1 wt%) was added using as a cocatalyst. The openings for the whole system were sealed with septums made of silicone rubber at ambient temperature and pressure. Prior to the reaction, the mixture was evacuated into vacuum and pumped by continuous Ar gas flow several times with stirring to remove O_2 and CO_2 dissolved in the solution. A 300 W xenon arc lamp equipped with 400 nm cut optical filter was used as a light source to trigger the photocatalytic reaction. The actual light intensity in the center of quartz reactor was measured by a visible light radiometer (made in the photoelectric instrument

Table 1 – Comparison of photocatalytic activities in hydrogen production over TiO_2-based photocatalysts.

Photocatalyst	Incident light	H_2 evolution rate (μmol h^{-1} g^{-1})	Reference
Sub-10 nm TiO_2 nanoparticle	Visible light	1954	[20]
Pure P25 (TiO_2)	Visible light	23	[25]
TiO_2 nanocrystal	Visible light	220	[26]
TiO_2 nanotube	83% Visible light	267	[27]
N–TiO_2 nanotube	83% Visible light	338.4	[27]
TiO_2 nanocrystal	Visible light	5841	[28]
H–TiO_2 nanocrystal	AM 1.5 G	10000	[29]
N-doped TiO_2 bowl nanoarray	Visible light	33	[30]
N-doped mesoporous TiO_2	Visible light	45	[31]
Black N–TiO_2	AM 1.5 G	150	[32]
N-doped TiO_2 microcrystallite	Visible light	211	[33]
Leaf-like N-doped TiO_2	Visible light	1410.5	[34]
N-doped TiO_2 nanofiber	AM 1.5 G	7557.9	[35]
N–O orbital hybridizated N–TiO_2 nanotube	**Visible light**	**10870**	**This work**

factory of Beijing Normal University, China). The focused light intensity on the liquid surface was maintained to 100 mW cm^{-2}. Gas product (H_2) was analyzed using an online gas chromatograph (SP7800, TCD, molecular sieve 0.5 nm, N_2 carrier, Beijing Keruida Limited) and the actual produced H_2 amount was quantified using an internal standard method. The procedures of photocatalytic hydrogen evolution for other N-doped TiO_2 samples and TiO_2 precursor were the same except with the corresponding catalysts.

Results and discussion

Fig. 1a and b shows the transmission electron microscope (TEM) images of N-doped TiO_2 nanotube, which show uniform and tubular structure with high quality. The length of nanotube is up to a few micrometers and the external diameter is about 13 nm in the enlarged TEM image in Fig. 1b. The wall thickness is only about 4 nm, and the ultrathin TiO_2 wall may provide more active sites and boost the catalytic performance. It should be pointed out that N-doping (1.85-N–TiO_2) will not change the morphology of the pristine TiO_2 template (Fig. S1). High resolution TEM (HRTEM) image in Fig. 1c displays distinct lattice fringes with a distance of 3.5 Å which can be indexed to the (101) plane of anatase phase TiO_2. The selected-area electron diffraction (SAED) pattern in Fig. 1d indicates that N-doped TiO_2 nanotube possesses high crystallinity, which implies high electron/holes separation ability in photocatalytic reactions [36]. The linear diffraction spots of (101) plane manifest that N-doping may intensively focus on the (101) surface. In order to further investigate the composition of N-doped TiO_2 nanotube, The energy-dispersive X-ray spectroscopy (EDS) test was obtained from the marked region in Fig. 1a, which confirms the existence of Ti, O and N elements with N mole ratio of 1.85 at.%. Therefore, we name this sample as 1.85-N–TiO_2 for convenience. Intuitively, N-doped TiO_2 nanotubes with varied N contents can be obtained by simply altering the amount of $NH_3 \cdot H_2O$ used as N precursor.

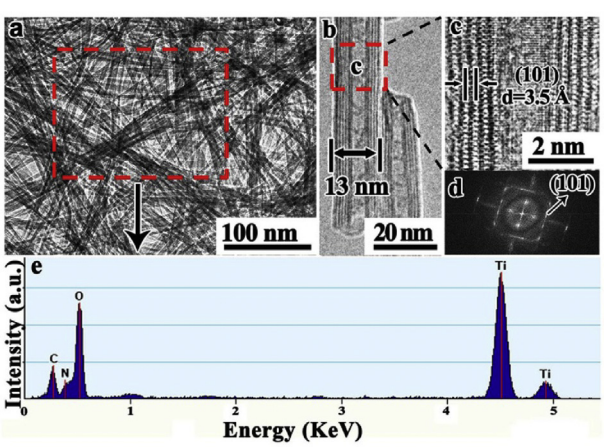

Fig. 1 – (a,b) TEM images and (c) HRTEM image of 1.85-N–TiO_2 nanotube. (d) The corresponding SAED patterns obtained from marked region c in Fig. 1b. (e) EDS spectrum of 1.85-N–TiO_2 nanotube obtained from the marked region in Fig. 1a.

As expected, N-doped TiO_2 nanotubes with N contents of 0.95, 1.04, 1.28 at.% were also obtained, as shown in Fig. S2. When N doping content was further increased to 2.51 and 3.53 at.%, the samples could not maintain the tubular structure and some agminated fragments appeared. This indicates that the largest N doping content in TiO_2 nanotube is about 1.85 at.%. Then, the surface areas of N-doped TiO_2 samples were examined by N_2 adsorption/desorption measurements, as shown in Fig. S3. The specific surface areas of the 0.95-N–TiO_2, 1.85-N–TiO_2 samples are 79 and 81 m^2 g^{-1}, respectively. The N-doped samples possess comparable specific surface areas and similar pore size distribution at around 3 nm (the insets in Fig. S3). The specific surface area is sharply depressed to 48 m^2 g^{-1} as N-doping content reaches 3.53 at.%, the less specific surface area is caused by the broken of the nanotube after excess N-doping, consistent with the TEM results (Fig. S2f).

In order to further investigate the phase structure for N-doped TiO_2 nanostructures, powder X-ray diffraction (XRD) measurements were performed. As indicated in Fig. 2a, all diffraction peaks for N-doped TiO_2 and TiO_2 precursor samples were matched well with that of anatase-phase TiO_2 (JCPDS card, NO. 71-1166). No impurity peaks including nitride or nitrogen are observed, indicating that N-doping could not changed the phase structure, even if N-doping content reaches 1.85 at.%. To further inspect the effects of N-doping on the lattice, the enlarged (101) diffraction peaks are shown in Fig. 2b and it is found that a clear shift to lower 2θ degree with the increasing of nitrogen content. The lattice extension for TiO_2 nanocrystals induced by N-doping reveals that N may supersede the O site [37].

The samples were further characterized by X-ray photoelectron spectroscopy (XPS) measurements to reveal the exact chemical states of N atoms in TiO_2 lattice. As shown in Fig. 3a, it can be seen that there are two main characteristic N 1s peaks for 1.85-N–TiO_2 nanotube around 394.1 and 399.5 eV, respectively. Obviously, no N 1s peaks can be observed for TiO_2 nanotube precursor in the same region. This clearly indicates that N has been successfully incorporated into the TiO_2 lattice after reaction. The peak located at 400.8 eV can be attributed to the N anion incorporated in the interstitial sites of O–Ti–O structure to form Ti–O–N–O bonds [38], and the peak at 399.5 eV belongs to the chemisorbed nitrogen species on the nanotube surface (essentially adsorbed NH_3) [16]. It should be pointed out that, the surplus N 1s peak located at 398.1 eV can be indexed to the N–Ti–N bond, accounting for the substituting N at oxygen sites (substitutional N) [39–41]. This kind of N species is recognized as a contributor for visible light absorption in N-doped TiO_2, because a continuous valence band composed of the hybrid orbits of N 2p and O 2p can be formed [14–16]. The peak located at 394.1 eV is far from N 1s, which may be derived from impurity. As a result, N-doping narrows the band gap of TiO_2 and extends the light absorption range for TiO_2 to visible light region [42]. The existence of N–Ti–N bond can also be proved by the XPS results of Ti 2p, in which the binding energies of Ti 2p shift from 459.1 to 458.4 eV with 0.7 eV discrepancy, as shown in Fig. 3b [43]. The peaks for O 1s also shift from 530.4 to 529.4 eV after N-doping (Fig. 3c), which is consistent with that of most reported [40,41]. The binding energy shift for Ti 2p and O 1s may be

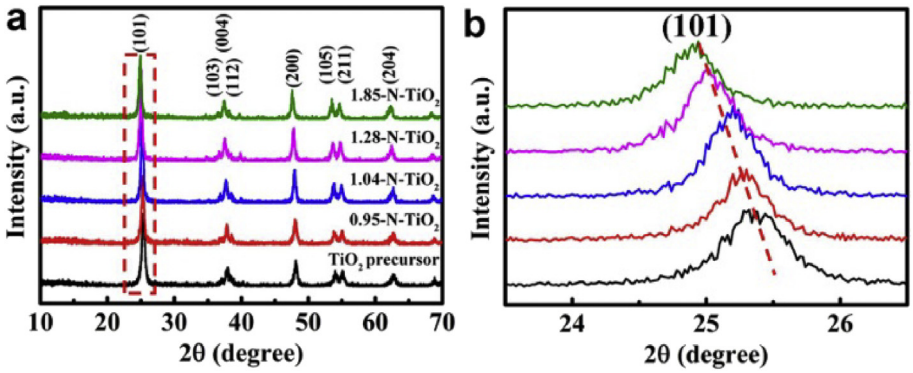

Fig. 2 – (a) XRD patterns of N-doped TiO_2 nanotubes with varied N-doping content. (b) The enlarged (101) peaks of N-doped TiO_2 samples.

caused by the lower electronegativity for N than O atom, therefore, N-doping in TiO_2 will change the charge distribution for Ti atom [44,45]. It is worth to note that there is no Ti^{3+} species detected in XPS spectrum, which clearly manifests that titanium nitride have not been formed.

Upon revealing the accurate crystal structure and constituent, we are now in a position to further investigate the band gap structure after N-doping in TiO_2 nanotube. The UV–vis diffuse reflectance spectrum measurements were firstly performed, as shown in Fig. S4 and the absorption spectra in the visible light region were shown in Fig. 3d. It can be seen that the absorption spectrum of pristine TiO_2 nanotube is cut off at 400 nm, which indicates a non-absorption feature in visible light region and a 3.20 eV band gap. With a slight N-doping, the 0.95-N–TiO_2 nanotube displays a wide absorption region range from 400 to 700 nm. As N-doping content increases to 1.85 at.%, the absorption property in visible light region is remarkably enhanced and widened, even to near infrared region. The huge absorption enhancement can be attributed to the narrowed band gap (from 3.2 to 2.77 eV) induced by N-doping (inset in Fig. 3d). The above UV–vis results of the N-doped TiO_2 nanotube imply their potential applications in the visible-light driven H_2 generation. Then, the valence band (VB) edges of 1.85-N–TiO_2 nanotube and pristine TiO_2 were also

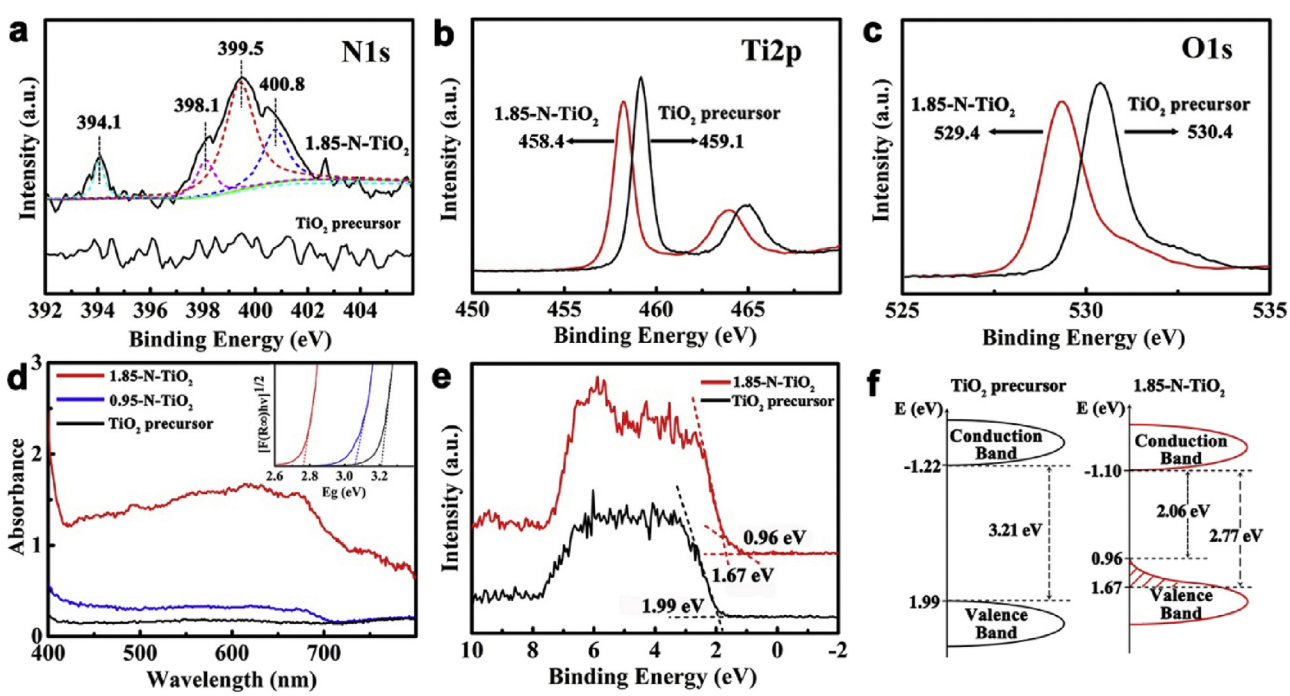

Fig. 3 – XPS spectrum measurement for 1.85-N–TiO_2 nanotube and TiO_2 precursor: (a) N 1s, (b) Ti 2p, and (c) O 1s. (d) UV–vis absorption spectra of the TiO_2 precursor, 0.95-N–TiO_2 and 1.85-N–TiO_2 nanotube in a range of 400–800 nm, respectively, the inset is the transition of Kubelka-Munk function. (e) Valence band spectra obtained from XPS. (f) The electronic band structures of TiO_2 precursor and 1.85-N–TiO_2 nanotube.

measured by their XPS valence band spectra, as shown in Fig. 3e. The valence band of 1.85-N–TiO_2 is valued by linear extrapolation of the peaks to the baselines, which displays a valence band edge position at 1.67 eV below the Fermi energy. After a careful observation, it is found that there is also a band tail red-shifted of the maximum energy deeply toward the vacuum level at about 0.96 eV. The band tail may be attributed to orbital hybridization between N 2p and O 2p, and greatly up-shift of the VB position and further narrow the band gap to 2.06 eV for 1.85-N–TiO_2 nanotube. Therefore, according to the band gap result, the conduction band (CB) minimum exists at about −1.10 eV, and the real band structure is shown in Fig. 3f. As a comparison, the VB and CB positions for pristine TiO_2 locate at 1.99 and −1.22 eV, respectively. The band structure for 1.85-N–TiO_2 and pristine TiO_2 clearly demonstrates that N-doping is an efficient approach to narrow the band gap of wide-band-gap semiconductors for visible light driven applications.

The effect of the orbital hybridization between N 2p and O 2p on the responsible sensitivity for the visible light has also been investigated by Zeta-potential measurements with an on-off cycle of white-light irradiation. As shown in Fig. 4a, with the light turning on and off, the pristine TiO_2 exhibits almost unchanged Zeta potentials at about 3 mV, which indicates that visible light could not excite electron/holes pairs, consistent with the UV–vis spectrum result. On the contrary, the Zeta potential turns to −1.4 mV for 1.85-N–TiO_2, which may be attributed to the decreased concentration of oxygen vacancy with N-doping [46]. Greatly different from the pristine TiO_2, as the visible light turning on, the Zeta potential of 1.85-N–TiO_2 nanotube down shifts to −4.5 mV with about a 3 mV discrepancy, which manifests that more photoelectrons are generated and successfully transferred to the surface of nanotube. The above results demonstrate convincingly that N-doping in TiO_2 triggers the absorption of visible light and simultaneously massive active electrons are produced. This is very favorable for the photocatalytic reduction process from $2H^+$ to H_2. To investigate the practical separation efficiency of electron/holes pairs under visible-light irradiation, steady-state photoluminescence (PL) spectroscopy measurements with the same amount of samples using a 420 nm excitation light have been conducted, as shown in Fig. 4b. It is found that the PL emission signals for N-doped samples are observed from 480 to 800 nm in the visible light region and a peak located at 520 nm, which are attributed to the free excitons at the band edge [14]. In contrast, no PL emission signal for undoped TiO_2 has been detected, which agrees with above-mentioned UV–vis and Zeta potential results (Figs. 3d and 4a). Besides, it is also found that 1.85-N–TiO_2 nanotube shows a lower emission peak around 520 nm than 0.95-N–TiO_2 sample, which indicates a less electron-hole recombination rate under the visible-light irradiation. Moreover, the generation and transport efficiency of the excited electrons of TiO_2 samples were also studied by comparable transient photocurrent measurements under visible-light irradiation (λ > 400 nm) at a bias potential of −0.3 V vs. Ag/AgCl, as shown in Fig. 4c. When the light was successively switched on and off, a series of signals were observed for pristine TiO_2, 0.95-N–TiO_2 and 1.85-N–TiO_2. Consistent with their PL results, 1.85-N–TiO_2 sample displays the largest photocurrent response under visible light, further verifies the large visible light absorption ability and low electron-hole recombination rate after N-doping in TiO_2.

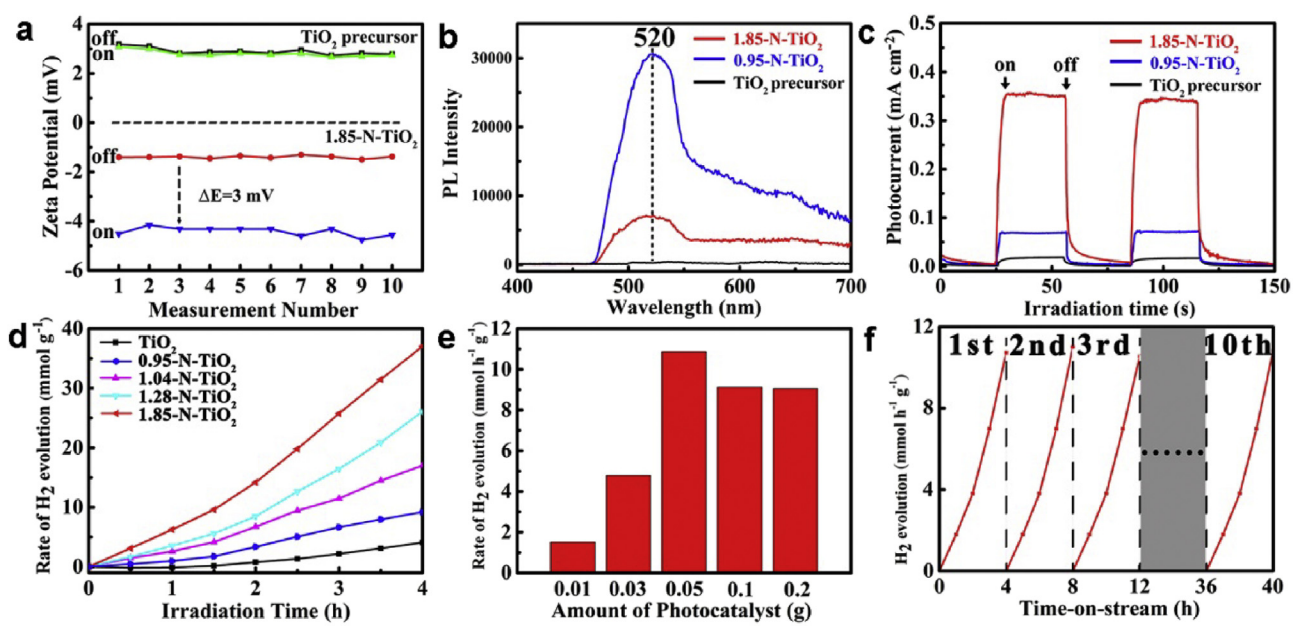

Fig. 4 – (a) Zeta potential measurements of 1.85-N–TiO_2 nanotube and pristine TiO_2 under a visible-light source. (b) Photoluminescence spectra using a 420 nm light as excitation light source. (c) Photocurrents versus time (*I-t*) curves of pristine TiO_2, 0.95-N–TiO_2 and 1.85-N–TiO_2 nanotubes under visible light illumination (λ > 400 nm) at a bias potential of −0.3 V vs. Ag/AgCl. (d) Visible-light driven H_2 generation with 0.1 g samples, the power densities are measured to be 100 mW cm^{-2}. (e) The photocatalytic H_2 production activities for 1.85-N–TiO_2 nanotube with different catalyst dosage. (f) The cycling stability results of photocatalytic H_2 production over 1.85-N–TiO_2 nanotube.

Afterwards, the photocatalytic H_2 production activities for N-doped TiO_2 and pristine TiO_2 samples were evaluated under simulative visible light irradiation (λ > 400 nm), in which $PtCl_6^{-2}$ was reduced to Pt nanoparticle as cocatalyst in the initial stage (Fig. S5). The experiment conditions for hydrogen production are similar with that of other TiO_2 based catalysts in Table 1. Fig. 4d shows the H_2 evolution amount versus reaction times, 1.85-N–TiO_2 nanotube shows a larger H_2 production rate of 9260 μmol h^{-1} g^{-1} than pristine TiO_2 (220 μmol h^{-1} g^{-1}) and other N-doped TiO_2 samples (2193 μmol g^{-1} h^{-1} for 0.95-N–TiO_2, 4709 μmol g^{-1} h^{-1} for 1.04-N–TiO_2, 6458 μmol g^{-1} h^{-1} for 1.28-N–TiO_2), which manifests that N-doping into TiO_2 lattice can really improve visible light driven H_2 production performance. In addition, the effect of hydrogen evolution activities on catalyst dosage for 1.85-N–TiO_2 nanotube was also investigated (Fig. 4e). The hydrogen evolution rate of 1.85-N–TiO_2 sample rapidly increases from 1510 μmol h^{-1} g^{-1} with 0.01 g sample to the maximum rate of 10870 μmol h^{-1} g^{-1} with 0.05 g sample, and then decreases to 9050 μmol h^{-1} g^{-1} with 0.2 g sample. With increasing the amount of catalyst, the absorbed photons gradually reach a saturation state and then cut off [47]. The photocatalytic hydrogen production activity for 1.85-N–TiO_2 nanotube is superior to that of other TiO_2 based catalysts all performed under visible-light and Pt as cocatalyst (Table 1). The comparison of hydrogen production performance can manifest that N-doping of TiO_2 is a highly efficient strategy to boost hydrogen production. The greatly enhanced hydrogen production performance should be enabled by two factors: *i*) the full absorption of visible light induced by the continuous valence band through N–O orbital hybridization in N-doped TiO_2. *ii*) The ultrathin TiO_2 shell boosts the catalytic active sites and shortens the distance of the carrier migrated to the surface to participate H_2 evolution reaction. Beside the high H_2 production rate, 1.85-N–TiO_2 nanotube also displays a satisfactory stability. As shown in Fig. 4f, no obvious decline for H_2 production rate has been detected in our cycling stability tests.

Conclusions

In summary, through a simple N-doping in TiO_2, a hybrid orbit composed of N 2p and O 2p has been realized experimentally for the first time. And it forms a consecutive intermediate valence band in the band gap and triggers the material's absorption for full visible-light spectrum. Specially, the as-obtained 1.85-N–TiO_2 nanotube exhibits a very high H_2 production rate (up to 10870 μmol h^{-1} g^{-1}) through a photocatalytic process under visible-light irradiation (λ > 400 nm). This catalyst design concept of introducing hybrid orbit into semiconductor enlightens a new way to realize full visible-light absorption for wide band gap semiconductor photocatalysts design in this field.

Acknowledgements

This work was financially supported in part by the Pandeng Plan Foundation (4095C5021820406), research start-up funding (4095C5021820441) of Hangzhou Normal University, Natural Science Foundation of Heilongjiang Province (B201603) and Zhejiang Provincial Natural Science Foundation (LY18E020010).

Appendix A. Supplementary data

Supplementary data to this article can be found online at https://doi.org/10.1016/j.ijhydene.2018.12.097.

Author contributions

The manuscript was written through contributions of all authors. All authors have given approval to the final version of the manuscript.

REFERENCES

[1] Fujishima A, Honda K. Electrochemical photolysis of water at a semiconductor electrode. Nature 2008;238:37–8.
[2] Shi W, Ma C, Wang H, Duan D, Sun Z, Yang S. A sea cucumber-like nanoporous TiO_2 modified by bimetal Pt-Au through the dealloying for water splitting. Int J Hydrogen Energy 2018;43:18850–62.
[3] Linsebigler A, Lu G, Yates J. Photocatalysis on TiO_2 surfaces: principles, mechanisms, and selected results. Chem Rev 1995;95:735–58.
[4] Zhao W, Liu J, Deng Z, Zhang J, Ding Z, Fang Y. Facile preparation of Z-scheme CdS-Ag-TiO_2 composite for the improved photocatalytic hydrogen generation activity. Int J Hydrogen Energy 2018;43:18232–41.
[5] Barrios C, Albiter E, Jimenez J, Tiznado H, Romo-Herrera J, Zanella R. Photocatalytic hydrogen production over titania modified by gold-Metal (palladium, nickel and cobalt) catalysts. Int J Hydrogen Energy 2016;41:23287–300.
[6] Chen X, Mao S. Titanium dioxide nanomaterials: synthesis, properties, modifications and application. Chem Rev 2007;107:2891–959.
[7] Preethi L, Antony R, Mathews T, Loo S, Wong L, Dash S, Tyagi A. Nitrogen doped anatase-rutile heterostructured nanotubes for enhanced photocatalytic hydrogen production: promising structure for sustainable fuel production. Int J Hydrogen Energy 2016;41:10327–34.
[8] Pei F, Xu S, Zuo W, Zhang Z, Liu Y, Cao S. Effective improvement of photocatalytic hydrogen evolution via a facile in-situ solvothermal N-doping strategy in N-TiO_2/N-graphene nanocomposite. Int J Hydrogen Energy 2014;39:6845–52.
[9] Bhowmick G, Noori M, Das I, Neethu B, Ghangrekar M, Mitra A. Bismuth doped TiO_2 as an excellent photocathode catalyst to enhance the performance of microbial fuel cell. l Int J Hydrogen Energy 2018;43:7501–10.
[10] Olowoyo J, Kumar M, Jain S, Shen S, Zhou Z, Mao S, Vorontsov A, Kumar U. Reinforced photocatalytic reduction of CO_2 to fuel by efficient S-TiO_2: significance of sulfur doping. Int J Hydrogen Energy 2018;43:17682–95.
[11] Mollavali M, Falamaki C, Rohani S. Efficient light harvesting by NiS/CdS/ZnS NPs incorporated in C, N-co-doped-TiO_2 nanotube arrays as visible-light sensitive multilayer photoanode for solar applications. Int J Hydrogen Energy 2018;43:9259–78.
[12] Livraghi S, Paganini M, Giamello E, Selloni A, Valentin C, Pacchioni G. Origin of photoactivity of nitrogen-doped

titanium dioxide under visible light. J Am Chem Soc 2006;128:15666–71.
[13] Presti L, Ceotto M, Spadavecchia F, Cappelletti G, Meroni D, Acres R, Ardizzone S. Role of the nitrogen source in determining structure and morphology of N-doped nanocrystalline TiO_2. J Phys Chem C 2014;118:4797–807.
[14] Yang C, Wang Z, Lin T, Yin H, Lü X, Wan D, Tao X, Zheng C, Lin J, Huang F. Core-shell nanostructured "Black" rutile titania as excellent catalyst for hydrogen production enhanced by sulfur doping. J Am Chem Soc 2013;135:17831–8.
[15] Park J, Kim S, Bard A. Novel carbon-doped TiO_2 nanotube arrays with high aspect ratios for efficient solar water splitting. Nano Lett 2006;6:24–8.
[16] Asahi R, Morikawa T, Ohwaki T, Aoki K, Taga Y. Visible-light photocatalysis in nitrogen-doped titanium oxides. Science 2001;293:269–71.
[17] Burda C, Lou Y, Chen X, Samia A, Stout J, Gole J. Enhanced nitrogen doping in TiO_2 nanoparticles. Nano Lett 2003;3:1049–51.
[18] Beranek R, Neumann B, Sakthivel S, Janczarek M, Dittrich T, Tributsch H, Kisch H. Exploring the electronic structure of nitrogen-modified TiO_2 photocatalysts through photocurrent and surface photovoltage studies. Chem Phys 2007;339:11–9.
[19] Huang B, Wey M. Properties and H_2 production ability of Pt photodeposited on the anatase phase transition of nitrogen-doped titanium dioxide. Int J Hydrogen Energy 2011;36:9479–86.
[20] Li L, Yan J, Wang T, Zhao Z, Zhang J, Gong J, Guan N. Sub-10 nm rutile titanium dioxide nanoparticles for efficient visible-light-driven photocatalytic hydrogen production. Nat Commun 2014;6:5881–91.
[21] Nakamura R, Tanaka T, Nakato Y. Mechanism for visible light responses in anodic photocurrents at N-doped TiO_2 film electrodes. J Phys Chem B 2004;108:10617–20.
[22] Batzill M, Morales E, Diebold U. Influence of nitrogen doping on the defect formation and surface properties of TiO_2 rutile and anatase. Phys Rev Lett 2006;96. 026103.
[23] Hoang S, Guo S, Hahn N, Bard A, Mullins C. Visible light driven photoelectrochemical water oxidation on nitrogen-modified TiO_2 nanowires. Nano Lett 2012;12:26–32.
[24] Ohsawa T, Henderson M, Chambers S. Epitaxial growth and orientational dependence of surface photochemistry in crystalline TiO_2 rutile films doped with nitrogen. J Phys Chem C 2010;114(14):6595–601.
[25] Xing M, Zhang J, Chen F, Tian B. An economic method to prepare vacuum activated photocatalysts with high photoactivities and photosensitivities. Chem Commun 2011;47:4947–9.
[26] Pan J, Liu G, Lu G, Cheng H. On the true photoreactivity order of {001}, {010}, and {101} facets of anatase TiO_2 crystals. Angew Chem Int Ed 2011;50:2133–7.
[27] Slamet, Tristantini D, Valentina, Ibadurrahman M. Photocatalytic hydrogen production from glycerol-water mixture over Pt-N-TiO_2 nanotube photocatalyst. Int J Energy Res 2013;37:1372–81.
[28] Zheng Z, Huang B, Lu J, Qin X, Zhang X, Dai Y. Hierarchical TiO_2 microspheres: synergetic effect of {001} and {101} facets for enhanced photocatalytic activity. Chem Eur J 2011;17:15032–8.
[29] Chen X, Liu L, Yu P, Mao S. Increasing solar absorption for photocatalysis with black hydrogenated titanium dioxide nanocrystals. Science 2011;331:746–50.
[30] Wang X, Long R, Liu D, Yang D, Wang C, Xiong Y. Enhanced full-spectrum water splitting by confining plasmonic Au nanoparticles in N-doped TiO_2 bowl nanoarrays. Nanomater Energy 2016;24:87–93.
[31] Liu S, Tang W, Lin W. Self-assembled ionic liquid synthesis of nitrogen-doped mesoporous TiO_2 for visible-light-responsive hydrogen production. Int J Hydrogen Energy 2017;42:24006–13.
[32] Cao Y, Xing Z, Shen Y, Li Z, Wu X, Yan X, Zou J, Yang S, Zhou W. Mesoporous black Ti^{3+}/N-TiO_2 spheres for efficient visible-light-driven photocatalytic performance. Chem Eng J 2017;325:199–207.
[33] Xiang Q, Yu J, Wang W, Jaroniec M. Nitrogen self-doped nanosized TiO_2 sheets with exposed {001} facets for enhanced visible-light photocatalytic activity. Chem Commun 2011;47:6906–8.
[34] Zhou H, Li X, Fan T, Osterloh F, Ding J, Sabio E. Artificial inorganic leafs for efficient photochemical hydrogen production inspired by natural photosynthesis. Adv Mater 2010;22:951–6.
[35] Han C, Wang Y, Lei Y, Wang B, Wu N, Shi Q. In situ synthesis of graphitic-C_3N_4 nanosheet hybridized N-doped TiO_2 nanofibers for efficient photocatalytic H_2 production and degradation. Nano Res 2015;8:1199–209.
[36] Zhou M, Yang P, Yuan R, Asiri A, Wakeel M, Wang X. Modulating crystallinity of graphitic carbon nitride for photocatalytic oxidation of alcohols. ChemSusChem 2017;10:4451–6.
[37] Yang X, Cao C, Erickson L, Hohn K, Maghirang R, Klabunde K. Photo-catalytic degradation of rhodamine B on C-, S-, N-, and Fe-doped TiO_2 under visible-light irradiation. Appl Catal B Environ 2009;91:657–62.
[38] Liu J, Han R, Zhao Y, Wang H, Lu W, Yu T, Zhang Y. Enhanced photoactivity of V-N codoped TiO_2 derived from a two-step hydrothermal procedure for the degradation of PCP-Na under visible light irradiation. J Phys Chem C 2011;115:4507–15.
[39] Sathish M, Viswanathan B, Viswanath R, Gopinath C. Synthesis, characterization, electronic structure, and photocatalytic activity of nitrogen-doped TiO_2 Nanocatalyst. Chem Mater 2005;17:6349–53.
[40] Chen X, Burda C. Photoelectron spectroscopic investigation of nitrogen-doped titania nanoparticles. J Phys Chem B 2004;108:15446–9.
[41] Wong M, Chou H, Yang T. Reactively sputtered N-doped titanium oxide films as visible-light photocatalyst. Thin Solid Films 2006;494:244–9.
[42] Irie H, Watanabe Y, Hashimoto K. Nitrogen-concentration dependence on photocatalytic activity of $TiO_{2-x}N_x$ powders. J Phys Chem B 2003;107:5483–6.
[43] Peng F, Cai L, Yu H, Wang H, Yang J. Synthesis and characterization of substitutional and interstitial nitrogen-doped titanium dioxides with visible light photocatalytic activity. J Solid State Chem 2008;181:130–6.
[44] Ye W, Chen S, Ye M, Ren C, Ma J, Long R, Wang C, Yang J, Song L, Xiong Y. $Pt_4PdCu_{0.4}$ alloy nanoframes as highly efficient and robust bifunctional electrocatalysts for oxygen reduction reaction and formic acid oxidation. Nano Energy 2017;39:532–8.
[45] Bai S, Yang L, Wang C, Lin Y, Lu J, Jiang J, Xiong Y. Boosting photocatalytic water splitting: interfacial charge polarization in atomically controlled core-shell cocatalysts. Angew Chem Int Ed 2015;54:14810–4.
[46] Yang Y, Gao P, Ren X, Sha L, Yang P, Zhang J, Chen Y, Yang L. Massive Ti^{3+} self-doped by the injected electrons from external Pt and the efficient photocatalytic hydrogen production under visible-Light. Appl Catal B Environ 2017;218:751–7.
[47] Li Q, Guo B, Yu J, Ran J, Zhang B, Yan H. Highly efficient visible-light-driven photocatalytic hydrogen production of CdS-cluster-decorated graphene nanosheets. J Am Chem Soc 2011;133(28):10878–84.